J. Fluid Mech. (1980), *vol.* 99, *part* 3, *pp.* 545–573
Printed in Great Britain

An experimental study of the effect of uniform strain on thermal fluctuations in grid-generated turbulence

By Z. WARHAFT

Sibley School of Mechanical and Aerospace Engineering,
Cornell University, Ithaca, New York 14853

(Received 4 June 1979 and in revised form 4 December 1979)

The effect of homogeneous strain on passive scalar fluctuations, and the resultant evolution of the scalar field when the strain is removed, is experimentally studied by passing thermal fluctuations in decaying grid turbulence through a four-to-one axisymmetric contraction. Using a *mandoline* (Warhaft & Lumley 1978*a*) to vary the scale size of the initial thermal fluctuations and hence the pre-contraction mechanical/thermal time-scale ratio, r, it is shown, for values of r greater than unity, that as r is increased so is the post-contraction thermal decay rate, i.e. the contraction does not cause the thermal-fluctuation decay rate to equilibrate to a constant value. In these experiments the post-contraction thermal decay rate is always greater than the pre-contraction decay rate, i.e. the contraction accelerates the thermal-fluctuation decay. Moreover, the mechanical/thermal time-scale ratio in the post-contraction region is driven further from unity. In terms of scale size the uniform strain has the effect of increasing the thermal length scale by an amount equal in value to the contraction ratio if the pre-contraction thermal length scale is comparable to that of the pre-contraction velocity scale. However, if the pre-contraction thermal length scale is smaller than the pre-contraction velocity scale then the effect of the contraction on the thermal scale is less marked. The contraction induces significant negative cross-correlation $\rho_{u\theta}$ between the longitudinal velocity u and thermal fluctuations θ even if the pre-contraction cross-correlation is close to zero. The magnitude of $\rho_{u\theta}$ and hence the post-contraction heat flux is varied and the coherence structure is studied. It is shown that the thermal-fluctuation decay rate is insensitive to the magnitude of the heat flux, the latter of which decays rapidly compared to the relatively slow decay of turbulence energy in the post-contraction region. It is also shown that $\rho_{u\theta}$ tends towards zero in this axisymmetric homogeneous flow at a faster rate than in isotropic turbulence. In accord with previous investigations, the return toward isotropy of the velocity field is very slow.

1. Introduction

The effect of applying a uniform strain to a turbulent field is of interest both to the wind-tunnel designer and the turbulence theoretician. From the design viewpoint a uniform strain in the form of a contraction upstream from the test section in a wind tunnel severely diminishes the turbulence intensity and hence dampens out unwanted disturbances. It was a desire for proper understanding of this effect that motivated the early analysis of Prandtl (1933) and the subsequent theoretical work of Taylor (1935)

0022-1120/80/4488-1640 $02.00

and Ribner & Tucker (1952), as well as the experiments of Uberoi (1956) and Mills & Corrsin (1959). The problem is, of course, of fundamental interest: uniformly straining an isotropic turbulent field is the simplest way of inducing anisotropy and an understanding of the dynamics of the development of the anisotropy as well as the subsequent return towards isotropy (if the mean strain is removed) is of basic importance when testing general turbulence theories and models. Insight into this problem is the first step toward an understanding of the more complex shear flows observed in nature and in the laboratory.

The problem of applying a mean strain to an isotropic turbulent field can be solved if the distortion is rapid, i.e. if the inertia and viscous forces arising from the turbulent motion can be neglected. For these assumptions the problem is linear (Batchelor 1953, p. 69). However, it is exceedingly difficult to achieve rapid distortion in a wind tunnel and neither the above-cited experimental work nor the results to be reported here come close to fulfilling the stringent requirements of the linear theory. There appears to be little theoretical advance in the nonlinear problem.

While the effect of straining isotropic turbulence is still poorly understood there has been more success in modelling the return to isotropy of homogeneous turbulence. Here the seminal ideas are due to Rotta (1951) who considered how the pressure–velocity correlation can affect a return to isotropy. Recently Lumley & Newman (1977) (see also Lumley 1978) have successfully modelled the post-contraction data of the experiments of Uberoi (1956) and Mills & Corrsin (1959) using second-order modelling procedures which have some of their origin in Rotta's early ideas. Schumann & Patterson (1978) and Schumann & Herring (1976) have also studied the return to isotropy of axisymmetric turbulence using spectral methods, the former using a direct spectral simulation which essentially integrates the Navier–Stokes equations, the latter using Kraichnan's (1959) direct-interaction approximation. Schumann & Herring (1976) also compare these two spectral methods and find that for high anisotropy the direct spectral simulation is superior while for low anisotropy the direct spectral simulation has statistical uncertainty and the direct interaction approximation is more accurate. However, this comparison has only been carried out for low Reynolds numbers to date.

The questions and problems associated with the velocity field can equally well be posed for a passive scalar field such as temperature. The effect of homogeneous strain on a scalar field and the subsequent return toward isotropy when the strain is removed is of vital importance to our understanding of atmospheric and industrial flows as well as to our interpretation of flow visualization studies. There is a paucity of data in this area; only one early experiment (Mills & Corrsin 1959) addresses this problem and in this experiment the thermal fluctuations were produced by heating a grid, which Warhaft & Lumley (1978*a*) found causes anomalous results.

Our broad objective here, then, is to study the effect of homogeneous strain, and the subsequent return towards isotropy when the strain is removed, for a passive scalar field in grid-generated turbulence.

Apart from the general need for such a study, this problem has specific and immediate interest to us. In a recent experimental study (Warhaft & Lumley 1978*a*) it was shown that in grid-generated turbulence the scalar fluctuation decay rate is a unique function of the relative input scale size of the velocity and temperature fluctuations. (The method of introducing the thermal fluctuations into the flow by means of a

mandoline will be reviewed in §§2 and 3 below.) If the initial mechanical/thermal length scale was increased then the decay rate of the thermal fluctuations relative to the velocity fluctuations increased. Further, there appeared to be no relaxation of the thermal decay rate to an equilibrium value in a tunnel of length equivalent to one eddy turn-over time, i.e. there does not appear to be an equilibrium value for the mechanical/thermal time-scale ratio, r, in such a flow in which the initial value of r is greater than unity (we were unable to set experimentally $r < 1$ using the *mandoline*). This result was contrary to expectation, which would have suggested that even for different initial thermal fluctuation decay rates the thermal decay rate should have asymptoted relatively quickly to a fixed value, a value which should have been independent of the initial conditions. It is interesting to note that this was the finding of Newman & Herring (1979) who used a Test Field Model approach to study this problem. (More recently their model has been modified to more closely predict the Warhaft & Lumley data (Herring & Newman 1979).)

The question raised by the above experiment was, then, is it possible to cause, by means of some disequilibrium, the mechanical/thermal time-scale ratio to relax to an equilibrium value? The use of an axisymmetric contraction to produce anisotropy, and hence disequilibrium, is one possible method of addressing this question and is the course taken here.

2. Experimental apparatus and procedure

The experiments to be described were conducted in a new wind tunnel built to the same dimensions as the tunnel used by Warhaft & Lumley (1978*a*) at the Pennsylvania State University, from here on referred to as the PSU tunnel. Thus the Cornell tunnel was vertically oriented with a 16×16 mesh length cross-section and streamwise extent of 180 mesh lengths, where the mesh length (M) of the biplane turbulence generating grid was 0·025 m. The grid bars were 0·476 cm square sectioned, giving a grid solidity of 0·34. The mean velocity was 6·43 m s^{-1}. The axisymmetric contraction with four to one velocity ratio was placed 60 mesh lengths from the grid, giving ample time for both the velocity and thermal fields to become homogeneous and close to isotropic. The contraction profile was a seventh-order polynomial, with symmetry at the midpoint and zero curvature and slope at the endpoints and is a scaled-down version of the primary contraction before the turbulence grid. The length of the contraction was 8 mesh lengths and the post contraction 8×8 mesh length section was 95 mesh lengths in extent. The walls in this section were slightly divergent to ensure a constant centerline mean speed of 25·7 m s^{-1} with the development of the boundary layer.

As for the PSU experiment the thermal field was generated by passing a current through a *mandoline* of fine wires oriented in one direction across the flow. The wire spacing was either one or two mesh lengths for the various experiments and the *mandoline* was located at various distances downstream from the grid in the pre-contraction region. The actual spacing and distances of the *mandoline* from the grid, varied to cause changes in thermal scale, will be given below in §3, where a comparison between the PSU tunnel and the Cornell tunnel will also be made. The *mandoline* wires were 0·321 mm diameter chromel-A. Measurements of velocity fluctuations taken without the grid but with the *mandoline* in the flow showed a low-level turbulence

spectrum, at worst 5%, and in the energy-containing range 3% of the spectrum measured with the grid in the flow. Since this is our measurement accuracy the effect of the *mandoline* on the velocity field was imperceptible. This was verified by taking velocity measurements downstream from the grid with and without the *mandoline* in the flow and no difference in spectral shape or level or in the velocity variance decay was observed for the two tests. We note that the *mandoline* solidity was very low, 0·011 and 0·0055 for the two *mandoline* configurations used, and that, although the *mandoline*-wire Reynolds number was 130 at ambient temperature, considerably higher than the von Kármán critical value of 40, at the film temperature of the heated wires, calculated to be approximately 230 °C, the Reynolds number should have been considerably reduced, to a value of about 50. As a further check of the effect of the *mandoline* on the flow some measurements with *mandoline* wires of half the diameter were made. Here the Reynolds number based on the film temperature should have been less than 40. The results obtained with the thinner wires gave the same results as those obtained with the thicker wires.

Velocity fluctuations were measured with DISA-type 55M constant-temperature bridges. The u (longitudinal velocity) and v (lateral velocity) components were measured with a 90° X-wire array with length-to-diameter ratio, l/d, of 200 and over heat ratio of 1·8. The wires were 3·2 μm diameter tungsten. Simultaneous temperature and u measurements were made with a parallel array of a 3·2 μm tungsten wire $l/d = 200$ and over heat 1·8 and a 1·27 μm diameter platinum wire with $l/d = 360$. The latter wire, which measured the temperature fluctuations, was used in conjunction with the same a.c. fast-response temperature bridge that was used in the PSU experiments.

The velocity signals were corrected for wire end effects and the temperature data were corrected for velocity contamination. Temperature and velocity signals were high-pass and low-pass filtered through Krohnhite-type 3342 filters; the bandwidth was generally 1 Hz to 5 kHz. The signals were recorded on digital magnetic tape and analysed on a PDP-11/34 mini-computer. Spectra and variances were calculated generally from 10^5 data points. Conventional FFT routines were used and spectra were smoothed by fitting a running second-order polynomial to the raw spectra by the method of least squares.

The reader is referred to Warhaft & Lumley (1978*a*) for further experimental protocol.

3. Review of heated *mandoline* experiments and comparison of the Cornell tunnel with the Pennsylvania State University tunnel

The essential finding of the PSU experiment was that the decay rate of temperature fluctuations in grid-generated turbulence is a unique function of the relative input scale size or wavenumber of the velocity and temperature fluctuations.

The velocity and thermal variance decay laws for grid-generated turbulence can be written in the forms

$$\overline{u^2}/U^2 = A(x/M)^{-n} \tag{1}$$

and

$$\overline{\theta^2}/T^2 = B(x/M)^{-m} \tag{2}$$

respectively. Here $\overline{u^2}$ is the longitudinal velocity variance, U is the mean velocity, x/M is the normalized downstream distance, $\overline{\theta^2}$ is the temperature variance, T is the

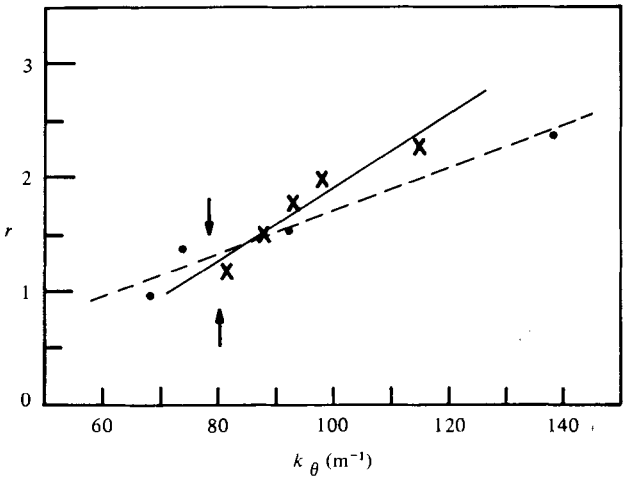

FIGURE 1. The mechanical/thermal time-scale ratio, r, *vs.* the peak of the three-dimensional temperature spectrum at $x/M = 53$. Dots are the PSU data, crosses are the present data; see table 1 for actual values. The downward-pointing arrow is the wavenumber at which the three-dimensional velocity spectrum peaked for the PSU measurements, the upward-pointing arrow is the velocity peak for the present work.

mean temperature (300 K for the experiments to be reported here) and A, B, n and m are constants. As the input length scale of the thermal fluctuations was decreased relative to the (fixed) input length scale of the velocity fluctuations, l, the decay exponent, m, increased. The decrease in length scale was effected by moving the *mandoline* away from the grid or by decreasing the spacing between the *mandoline* wires and was determined from the peak in the three-dimensional temperature spectrum, k_θ ($k_{\max}$ in Warhaft & Lumley 1978*a*). Defining a mechanical/thermal time-scale ratio, r, by

$$r = \tau/\tau_\theta = (\overline{q^2}/\epsilon)/(\overline{\theta^2}/\epsilon_\theta), \tag{3}$$

where $\overline{q^2}$ is twice the turbulence kinetic energy and where

$$\epsilon = -\tfrac{1}{2}(d\overline{q^2}/dt) \tag{4}$$

and

$$\epsilon_\theta = -\tfrac{1}{2}(d\overline{\theta^2}/dt) \tag{5}$$

are the energy and thermal dissipation rates respectively, then $r = m/n$. Thus a higher value of m yields a higher r.

Figure 1 is a plot of r *versus* k_θ and compares the PSU data with the present data at $x/M = 53$. Also shown is the wavenumber at which the three-dimensional velocity spectra peaked. The data compare reasonably well; differences and possible reasons for the differences will be discussed below. The new data, taken for the region before the contraction where the turbulence field is almost isotropic, are essentially the same as for some preliminary measurements done with the present tunnel but with a constant-area test section rather than with the contraction in place at $x/M = 60$. Table 1 summarizes the *mandoline* configurations as well as the values of k_θ, m and n for the present experiments. In table 1 and in the following description the *mandoline* configuration is specified by two numbers in parenthesis; the first is the distance of the *mandoline* from the grid and the second is the spacing between the wires. Thus,

	k_θ (m^{-1}) from three-dimensional spectrum at $x/M = 53$		Decay exponent m		$r = m/n$	
Mandoline configuration	No contraction	With contraction	No contraction	With contraction	No contraction	With contraction
(2, 2)	80	81	1·6	1·8	1·2	1·2
(5, 1)	not measured	88		2·25		1·5
(15, 2)	90	93	2·4	2·7	1·8	1·8
(10, 1)	98	98	2·7	3·0	2·0	2·0
(15, 1)	not measured	115		3·5		2·3
	k (m^{-1})		n			
Velocity field	80	80	1·35	1·5		

TABLE 1. Peak of three-dimensional temperature and velocity spectra and the decay exponent values for the pre-contraction region and for some preliminary experiments done with a test section of uniform cross-section (no contraction).

mandoline at (5, 1) means the *mandoline* is 5 mesh lengths from the grid and the spacing is 1 mesh length, where the mesh length is that of the velocity grid. Note (table 1) that the contraction has the effect of slightly increasing the pre-contraction thermal decay exponent compared to measurements done without the contraction but, since n is also increased, r before the contraction was the same as for experiments done without the contraction. The contraction did not appear to affect k_θ (table 1). The actual plots of temperature variance decay and of the three-dimensional spectra from which figure 1 was derived will be discussed in §4.2 (figures 10, 11, and 16).

The PSU data, which were reported for $x/M = 80$ (Warhaft & Lumley 1978*a*, figure 16) have been transformed to $x/M = 53$ for comparison with the present data (figure 1) by shifting k_θ to higher wavenumbers according to $(lk_\theta)_{53} = (lk_\theta)_{80}$, where the subscripts refer to the distance in mesh lengths from the grid. It was found in the PSU experiments, and verified again here, that the peaks of the temperature spectra increase according to the above relation (Warhaft & Lumley 1978*a*, figure 20).

Figure 1 shows that although the salient characteristics of the PSU and Cornell data compare well, there are some differences between the two sets of results; the smallest r that could be achieved in the present experiment was 1·2 compared with 1·0 for the PSU measurements (moving the *mandoline* closer to the grid than 2 mesh lengths did not decrease r below 1·2) and that the slope of the line suggested by the relation between r and k_θ is greater for the present work. These differences are probably due to a slight difference in the velocity fields for the two tunnels. While the peak of the velocity spectra occurs at approximately the same wavenumbers, 78 m^{-1} for the PSU results and 80 m^{-1} for the present work, the intensity of the velocity fluctuations for the present tunnel were lower than for the PSU tunnel, the respective decay laws being $\overline{u^2}/U^2 = 0{\cdot}1225(x/M)^{-1{\cdot}34}$ (PSU) and $\overline{u^2}/U^2 = 0{\cdot}08(x/M)^{-1{\cdot}35}$ (present work). The reason why the intensity in the Cornell tunnel is lower is not clear; we attempted to duplicate the grid structure of the PSU tunnel. It should be noted that the turbulence levels of the Cornell tunnel are closer to those of the tunnels used by Comte-Bellot & Corrsin (1966) and Yeh & Van Atta (1973) for comparable grid Reynolds numbers.

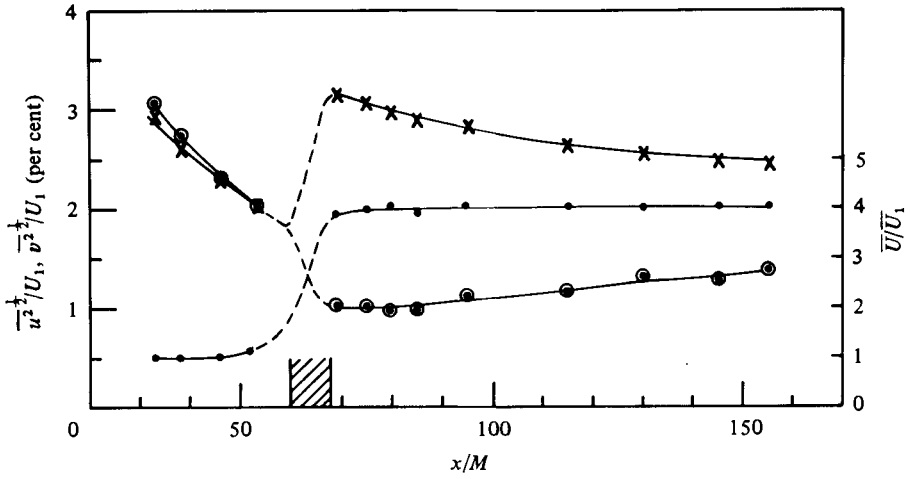

FIGURE 2. The effect of the contraction on the velocity fluctuations and mean velocity. ⊙; $\overline{u^2}^{\frac{1}{2}}/U_1$; ×, $\overline{v^2}^{\frac{1}{2}}/U_1$; •, U/U_1. The grid is at $x/M = 0$ and the contraction is from $x/M = 60$ to $x/M = 68$.

Finally we note that the *mandoline* configurations used for this experiment are different from those used at PSU. Here the maximum distance of the *mandoline* from the grid was 15 mesh lengths while for the PSU data it was 20 mesh lengths. The reason for this was to allow the thermal field as much time as possible to become homogeneous before the first measurement (at $x/M = 33$) and thus for the thermal decay characteristics to become well established before the contraction at $x/M = 60$. It must be noted that the *mandoline* configuration is immaterial to the trend of figure 1. Thus it was found in preliminary measurements that for the *mandoline* at (10, 2) a similar decay rate and k_θ was observed as for the *mandoline* at (5, 1). The essential characteristic of the *mandoline* is that it provides a method of varying the input scale of the thermal fluctuations.

4. The results

4.1. *The velocity data*

Figure 2 shows the normalized r.m.s. longitudinal velocity, $\overline{u^2}^{\frac{1}{2}}/U_1$, the normalized r.m.s. lateral velocity $\overline{v^2}^{\frac{1}{2}}/U_1$ and the mean velocity U/U_1, where U_1 is the mean velocity before the contraction, plotted as a function of x/M. The return towards isotropy of the velocity fluctuations after the contraction is extremely slow; this is in conformity with the previous data of Uberoi (1956) and Mills & Corrsin (1959).

Table 2 lists the r.m.s. ratios u_2/u_1, v_2/v_1, $(v_2/u_2)/(v_1/u_1)$ and q_2/q_1, where the subscripts 1 and 2 refer to the r.m.s. values of the velocity components just prior to the contraction and just after the contraction respectively and q is the r.m.s. of twice the turbulence energy per unit mass, taken here as $(\overline{u^2} + 2\overline{v^2})$. Also listed in table 2 are the same ratios computed from the measurements of Uberoi (1956) and Mills & Corrsin (1959) as well as the theoretical predictions of the linear theory of Ribner & Tucker (1952). It should be noted that in both the experiments of Uberoi and of Mills & Corrsin the velocity field does not reach isotropy in the pre-contraction region since

Ratio	Ribner & Tucker (1952) (linear theory)	Mills & Corrsin (1959) $R_m = 6600$	Uberoi (1956) 4:1 contraction ratio $R_m = 3710$	$R_m = 6150$	$R_m = 12300$	Present study $R_m = 9700$
u_2/u_1	0·4	0·7	0·55	0·55	0·5	0·53
v_2/v_1	1·5	1·4	1·6	1·5	1·4	1·63
$\frac{v_2/u_2}{v_1/u_1}$	3·8	2·0	2·9	2·7	2·8	3·1
q_2/q_1	1·2	1·2	1·35	1·3	1·2	1·36

TABLE 2. Various post- to pre-contraction velocity ratios (after Mills & Corrsin 1959). R_m is the mesh Reynolds number $= U_1 M/\nu$.

the contraction is placed relatively close to the grid (21 and 42 mesh lengths in the work of Uberoi and 18 mesh lengths in the work of Mills & Corrsin). Uberoi (1956) defines the beginning of his contraction as the point at which u and v equalize, which is slightly downstream from the geometrical beginning. In the present work approximate isotropy is achieved before the contraction. This is probably due to the effect of having the contraction relatively far downstream from the grid (60 mesh lengths) as well as to the slight straining of the velocity field that must occur before the geometrical beginning of the contraction. Both these aspects enhance $\overline{v^2}$ relative to $\overline{u^2}$.

The present results (table 2) are within about 10% of the Uberoi (1956) results. None of the experimental results are in good agreement with the rapid-distortion theory of Ribner & Tucker (1952). As discussed by Batchelor (1953), for linear theory to hold $\overline{u^2}^{\frac{1}{2}}/U \ll l/D$, where l is the length scale of the turbulence and D is the length of the distorting element. In our experiment these two ratios are of the same order of magnitude. It is evident that the requirements of linear theory are very difficult to meet; for the pre-contraction turbulence level and scale size of the present experiment the length of the contraction would have to be less than one mesh length and separation would certainly occur.

Figure 3 compares the u spectra and figure 4 compares the v spectra before and after the contraction. These spectra have been plotted as a function of frequency and have been normalized so that the areas under the curves are equal. Thus changes in shape rather than amplitude are being compared. The u spectrum (figure 3) is more affected by the contraction than the v spectrum (figure 4) which hardly changes in form. This is in conformity with previous experimental findings and with the rapid-distortion theory (Ribner & Tucker 1952), which show that the u spectrum should peak at a higher frequency after passing through the contraction.

Figure 5 shows the three-dimensional normalized velocity spectra before the contraction where the flow is close to isotropic and thus the one-dimensional spectra can be transformed into a three-dimensional spectrum according to the relationship (Tennekes & Lumley 1972)

$$E(k) = -\tfrac{1}{2}k\,d\phi(k)/dk,$$

where $\phi(k_1) \equiv \phi_u(k_1) + 2\phi_v(k_1)$ and $\phi_u(k_1)$ and $\phi_v(k_1)$ are the one-dimensional power spectra of u and v respectively and

$$\int_0^\infty \phi(k_1)\,dk_1 \equiv \overline{q^2}.$$

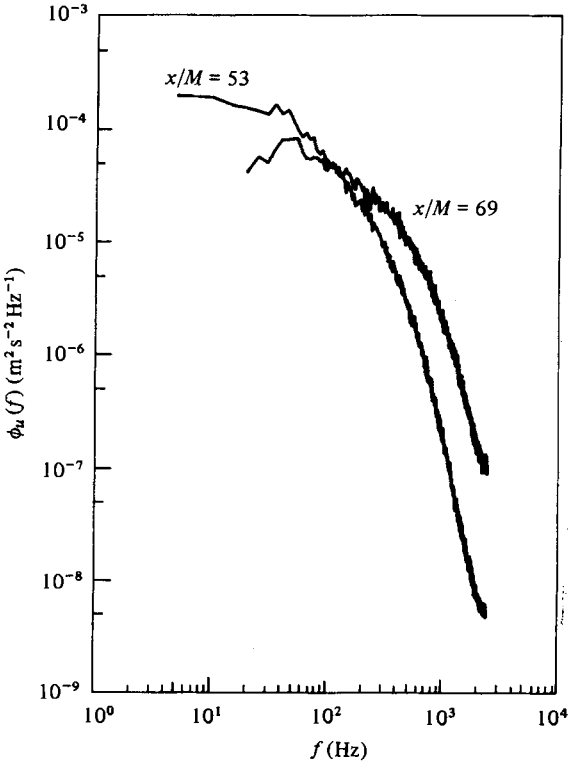

FIGURE 3. One-dimensional u (longitudinal velocity) spectra before and after the contraction normalized so that the variances of the two spectra are the same.

The spectra have been normalized by division by the local values of $\overline{u^2}$ and l, where $l \equiv (\overline{u^2})^{\frac{3}{2}}/\epsilon$ and ϵ has been calculated by differentiating the velocity decay law (equation (4)). At $x/M = 53$, l was found to be $1{\cdot}4 \times 10^{-2}$ m from the velocity decay law and thus compared well with the length scale deduced from the peak of the unnormalized three-dimensional velocity spectrum, which was 80 m^{-1} giving a length of $1{\cdot}25 \times 10^{-2}$ m. Thus the spectrum of figure 5 peaks at $kl = 1{\cdot}1$. By contrast, the PSU normalized three-dimensional spectrum (figure 5, Warhaft & Lumley 1978*a*) peaked at $kl = 1{\cdot}5$ since the higher turbulence intensity of that tunnel indicated that l, deduced from the velocity decay law, was greater than l deduced from the three-dimensional spectrum, the latter of which peaked at approximately the same wavenumber as for the Cornell tunnel. In other respects the PSU velocity spectra are quite similar to the pre-contraction spectra of the Cornell tunnel.

The three-dimensional spectra of figure 5 can only be formed from the one-dimensional spectra if the flow is isotropic, which is approximately the case before the contraction but definitely not the case after the contraction. Thus in order to compare velocity scales after the contraction with those before the contraction the one-dimensional spectra were plotted in the form $k_1\phi(k_1)$ versus k_1, where $k_1 = 2\pi f/U$ and U is the local velocity, i.e. 6·43 m s^{-1} before the contraction and 25·72 m s^{-1} after the contraction. It has been shown by Lumley & Panofsky (1964) that for an exponential correlation function the peak of the $k_1\phi(k_1)$ spectrum determines the integral length

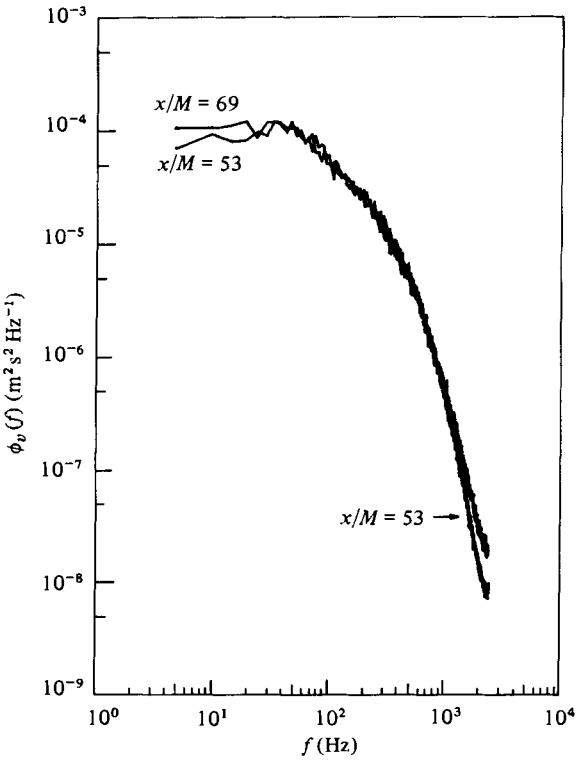

FIGURE 4. One-dimensional v (lateral velocity) spectra before and after the contraction normalized so that the variances of the two spectra are the same.

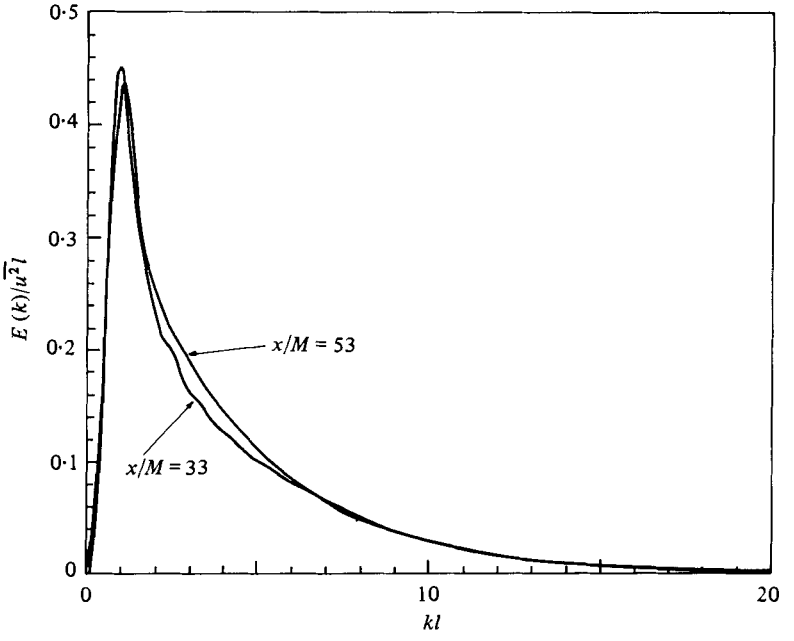

FIGURE 5. Normalized three-dimensional velocity spectra for the approximately isotropic region before the contraction.

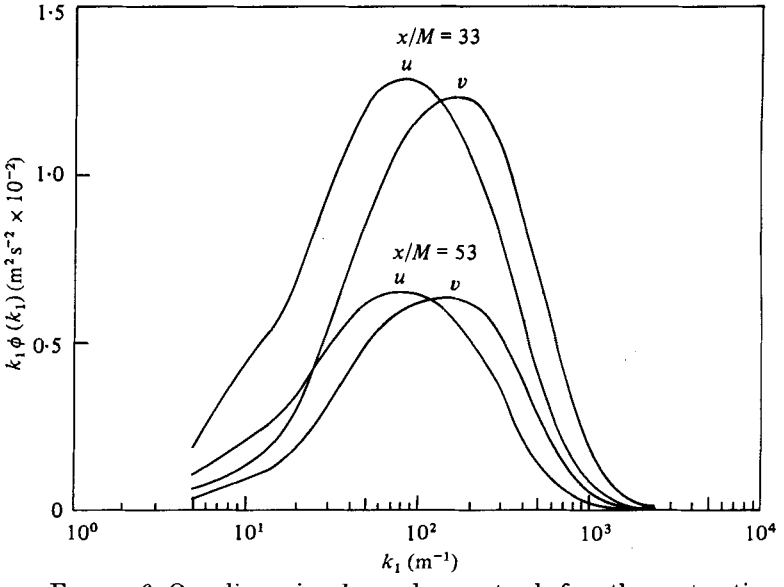

FIGURE 6. One-dimensional u and v spectra before the contraction.

scale. While the form of our correlation functions could only very crudely be modelled as exponential (an exponential correlation function transforms to a spectrum with a -2 power-law decay), we are not using this representation to deduce integral scales but only to compare relative changes in length scales. Since the one-dimensional spectra $\phi(k_1)$ we are comparing are similar in form, this limited interpretation of $k_1\phi(k_1)$ is justified. Figure 6 shows the u and v one-dimensional spectra plotted in this way for the region before the contraction and figure 7 and 8 show the u and v spectra respectively, for the region after the contraction. The wavenumber at which the u spectrum peaks only diminishes slightly after passing through the contraction (figures 6 and 7) while the v spectrum peaks at a post-contraction wavenumber of about 0·25 the pre-contraction wavenumber (figures 6 and 8). Thus the geometrical effect of the contraction is only slightly felt by the u component while for the v component the length scale is increased by the contraction ratio. These findings are in qualitative agreement with the experiments of Uberoi (1956) and Mills & Corrsin (1959).

Figures 7 and 8 also show the change in spectral peaks as x/M is increased for the region downstream of the contraction. Contrary to what occurs in decaying isotropic turbulence where length scales increase with x/M, here the u component scale decreases, and so also does the v component scale, but to a lesser extent, as the turbulence energy decays. The decrease in the u scale size is to be expected since, as figure 2 shows, the u component is not decaying but is receiving energy from the v and w components. The reason for the slight decrease in scale size of v (figure 8) is not clear.

4.2. *The temperature data*

(*a*) *The variance characteristics.* Figure 9 shows the temperature variance decay for four different *mandoline* configurations. The temperature variance has been normalized with the square of the absolute temperature, T^2. We note that some authors (e.g. Mills & Corrsin 1959) normalize the temperature variance with ΔT, the mean temperature

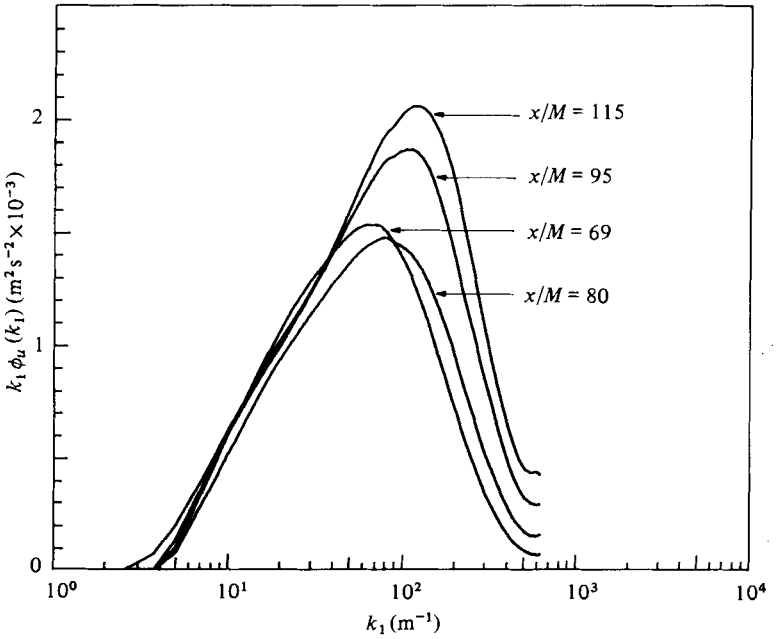

FIGURE 7. One-dimensional u spectra after the contraction.

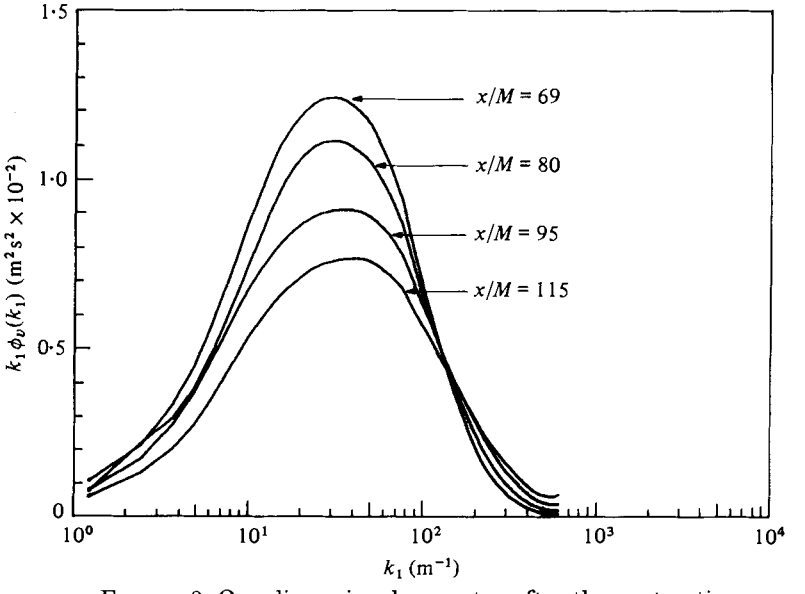

FIGURE 8. One-dimensional v spectra after the contraction.

rise across the heat generating element. Our choice of T was to facilitate comparison between decay experiments done with different initial $\overline{\theta^2}$ to be discussed below. Since T remained essentially constant (300 K) for the different experiments, the ordinate is proportional to $\overline{\theta^2}$. This normalization also allows easier comparison

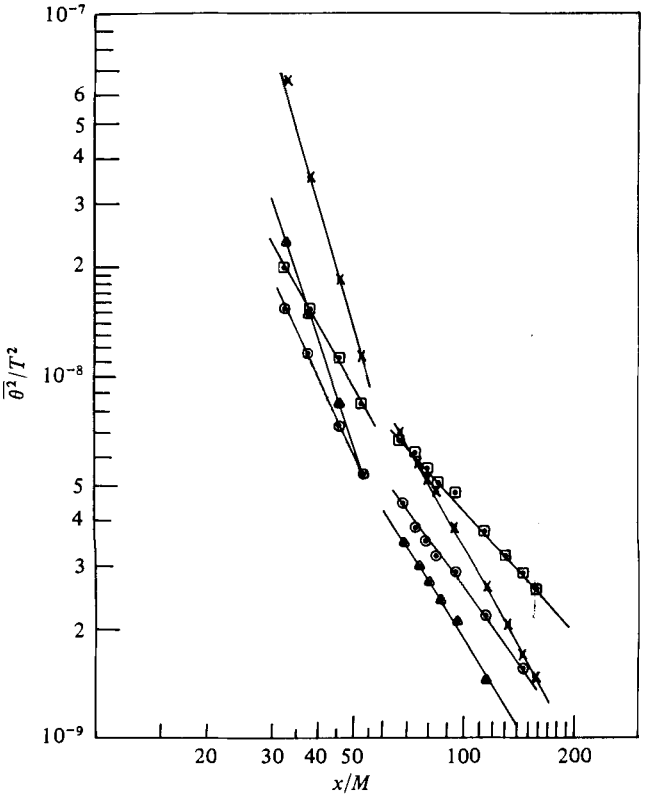

FIGURE 9. Decay of temperature variance. ⊡, *mandoline* at (2, 2); ⊙, *mandoline* at (5, 1); △, *mandoline* at (10, 1) ×, *mandoline* at (15, 1).

with our earlier work (Warhaft & Lumley 1978*a*, *b*) which was normalized in the same way. The origin ($x/M = 0$) for figure 9 was taken at the grid. The contraction alters the rate of decay of temperature variance, but its decay rate after the contraction is a function of its decay rate before the contraction. The temperature variance decay can be described well by means of a power-law decay for the post-contraction region as well as for the pre-contraction region. We will refer to the decay exponent before and after the contraction as m_b and m_a respectively. It must be noted however that m_a is only useful for comparing results of this experiment, it has no absolute significance since its value is dependent on where the contraction is located relative to the origin (grid). Table 3 lists m_a and m_b for the five different *mandoline* configurations. (The fifth *mandoline* configuration (15, 2), not shown in figure 9, will be discussed below.)

In order to compare the evolution of the strained (post-contraction) thermal field with that of an unstrained field that would be obtained the same distance downstream from the grid but without the contraction it is more appropriate to use dimensionless time, tU_1/M, rather than distance, x/M, as the reference (Mills & Corrsin 1959). Figure 10 is such a plot of the data of figure 9. Also included in this figure is a decay for the *mandoline* at (2, 2) done without the contraction, showing, as noted above (see table 1), that the contraction has the effect of slightly increasing the thermal

Mandoline configuration	*Mandoline* current (A)	r	m_b	m_a	m_{at}	k_b (m^{-1})	k_a (m^{-1})	r_a at $x/M = 85$	r_a at $x/M = 145$
(2, 2)	2·5	1·2	1·8	1·13	3·2	61	14·5	1·88	3·54
(5, 1)	2·6	1·5	2·25	1·43	4·0	78	18	2·38	4·48
(15, 2)	1·2	1·8	2·7	1·60	4·6	100	24	2·67	5·01
(10, 1)	1·9	2·0	3·0	1·68	4·9	115	34	2·8	5·25
(15, 1)	1·6	2·3	3·5	1·9	5·4	200	110	3·17	5·96

TABLE 3. The pre-contraction time-scale ratio r, the pre- and post-contraction decay exponents m_b and m_a (and m_{at}) respectively, the peaks of the one-dimensional spectra before the contraction, k_b, at $x/M = 53$, and after the contraction k_a, at $x/M = 69$, and the post-contraction time-scale ratio, r_a, at $x/M = 85$ and $x/M = 145$. Also included is the *mandoline* current for each configuration. The resistance of a heated *mandoline* wire was approximately 5·6 Ω. For the *mandoline* (15, 2), high current (4·5 A) there was no measurable difference compared to the parameters for the low *mandoline* current at (15, 2) (1·2 A) tabulated above.

decay rate upstream of the contraction apart from drastically increasing it after the contraction. From this figure it is evident that the contraction has the effect of accelerating the decay of the thermal fluctuations. This was also found by Mills & Corrsin (1959) for their single realization of thermal decay through a contraction using a heated grid to produce the thermal fluctuations. Mills & Corrsin (1959) also did a crude analysis of the effect of a contraction on thermal fluctuations. They assume instantaneous distortion of a homogeneous thermal field under the action of a uniform mean strain. For a contraction ratio of 4:1, their calculations for the ratio of the pre- to post-contraction thermal variance decay rate yields a value of 0·67. From figure 10 we calculate the ratio $(d\overline{\theta^2}/d\tau)_{59}/(d\overline{\theta^2}/d\tau)_{65}$ to vary from 0·5 (*mandoline* at (2, 2)) to 0·8 (*mandoline* at (15, 1)). Here the subscripts refer to the dimensionless time, $\tau = tU_1/M$, at which the derivatives were evaluated. $\tau = 59$ is just prior to the contraction and $\tau = 65$ is just after it.

The power-law decay is still well preserved for the thermal fluctuation decay after the contraction in the time plot of figure 10. This decay exponent will be referred to as m_{at} and is listed in table 3. The ratio m_a/m_{at} for each experiment was 0·35 to within a few per cent. Table 3 also lists the post-contraction mechanical/thermal time scale ratio, r_a, for each experiment. Here, as for the pre-contraction region, r_a has been calculated from equation (3) using the data from figures 2 and 9. It is evident that the contraction has the effect of driving the mechanical/thermal time-scale ratio further away from unity. The ratio r_a/r, where r is the pre-contraction time-scale ratio, for the region just after the contraction, varies from 1·57 (*mandoline* at (2, 2)) to 1·38 (*mandoline* at (15, 1)).

The four different decay experiments of figures 9 and 10 were done with very low thermal fluctuation intensities. This was to keep the initial cross-correlation between u and θ ($\rho_{u\theta}$) at a low value ($\sim -0{\cdot}05$).† It will be shown that the contraction induces

† The negative correlation exists because locally, at various positions along the *mandoline* wire, whisps of fast air will cause cooling (and vice versa) producing a net negative correlation between u and θ, even though the wire as a whole is working at a constant power input. The higher the *mandoline* wire overheat, the higher the magnitude of $\rho_{u\theta}$. However, for the four experiments of figures 9 and 10 the velocity field was the same as that measured for the flow without thermal fluctuations and thus temperature was a passive additive. We note also that $g/T(\overline{u\theta}) \ll \epsilon$.

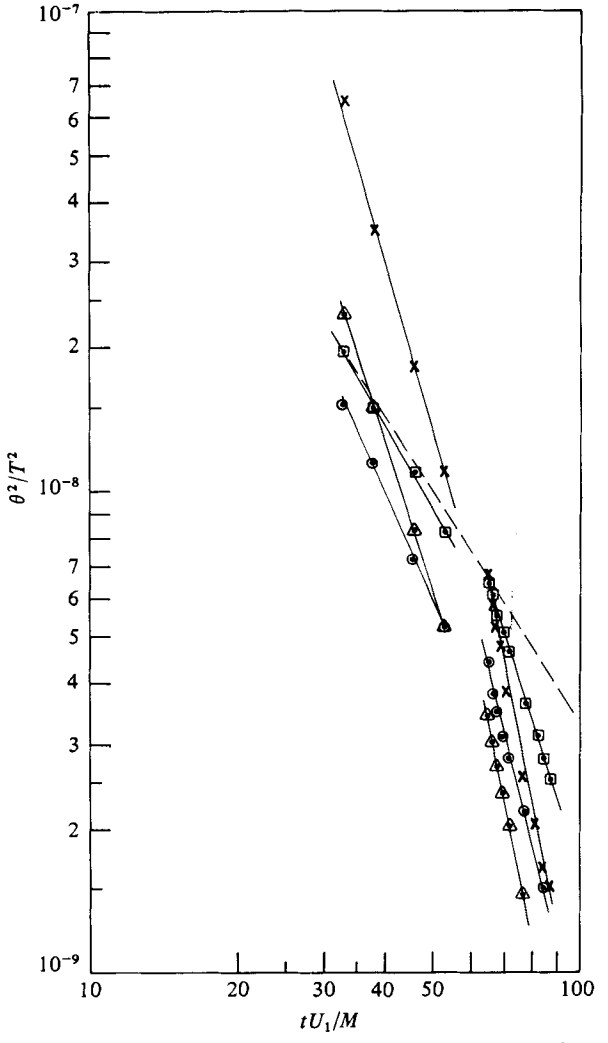

FIGURE 10. Same data as figure 9 but with non-dimensional time tU_1/M as absicissa. Dashed line is the decay for *mandoline* at (2, 2) without the contraction.

large negative $\rho_{u\theta}$ and in our initial experiments we were aiming to study flow conditions in which the effect of heat flux could be neglected. However, figure 11 shows that the thermal decay characteristics are in fact remarkably independent of initial fluctuation intensity (and hence heat flux). In these realizations for the *mandoline* at (15, 2) the initial fluctuation variance, $\overline{\theta^2}/T^2$, was varied by nearly a factor of 100 and there is no discernible difference in m_b or m_a for the two cases. This is in spite of extremely high magnitude of $\rho_{u\theta}$ induced by the contraction, and hence the production of some buoyancy in the immediate post-contraction region, for the case with the higher thermal fluctuations (see §4.2(*c*) below). Also plotted in this figure is the thermal decay, done for the case of higher heating, without the contraction.

Figure 12 is a plot of m_a (and m_{at}) as a function of m_b for the five *mandoline* experiments. There is a linear dependence between m_b and m_a (or m_{at}).

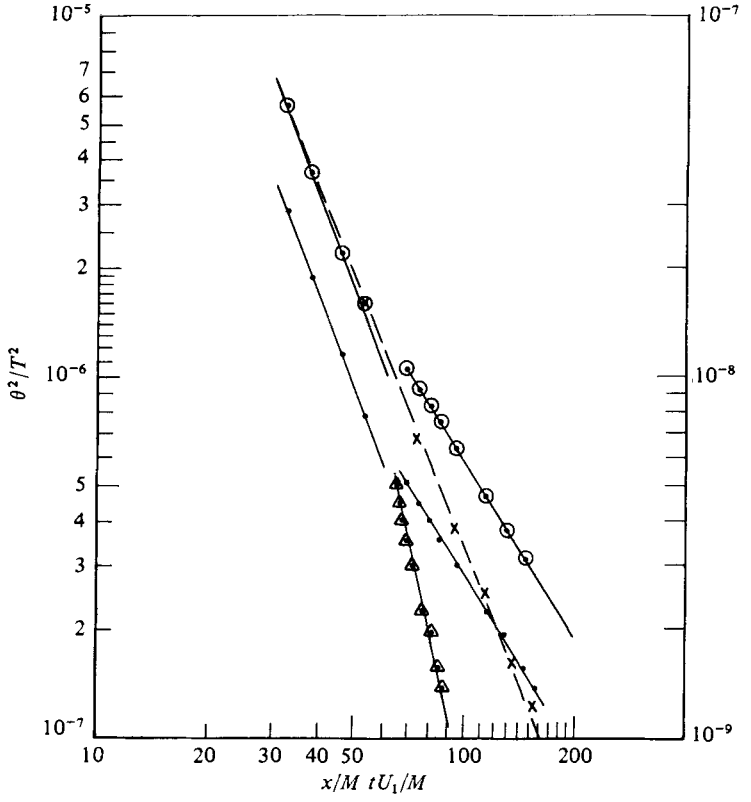

FIGURE 11. Decay of temperature variance for *mandoline* at (15, 2). ⊙, high heating (4·5 A) (left-hand scale) as function of x/M; ×, high heating without the contraction as function of x/M; ·, low heating (1·2 A) (right-hand scale) as function of x/M; △, low heating (1·2 A) as function of tU_1/M.

(*b*) *The spectral characteristics.* Figures 13, 14 and 15 show the pre- and post-contraction one-dimensional temperature spectra plotted as a function of frequency for the *mandoline* at (5, 1), (10, 1) and (15, 1) respectively. As for the velocity spectra, these spectra have been normalized so that the areas under the curves are equal. It is evident from figures 13, 14 and 15 that as the time-scale ratio increases the relative forms of the spectra before and after the contraction change. For the *mandoline* at (5, 1), $r = 1{\cdot}5$, the forms of the spectra before and after the contraction are quite similar (figure 13) while for the *mandoline* at (15, 1), $r = 2{\cdot}3$, the spectrum after the contraction has higher frequency components than before the contraction (figure 15) (note for these spectra a higher digitization rate has been used for the post-contraction data). Figure 14, $r = 2$, appears to be approximately half-way between the above-mentioned cases. For the remaining two experiments, the *mandoline* at (2, 2) and (15, 2), $r = 1{\cdot}2$ and $1{\cdot}8$ respectively, the spectra before and after the contraction (not shown here) were similar in form, i.e. they were like the case for the *mandoline* at (5, 1), figure 13.

Figure 16 compares the position of the peaks of the three-dimensional temperature spectra in the pre-contraction region at $x/M = 53$. k_θ, table 1, was taken from these curves, which were computed by transforming the one-dimensional temperature

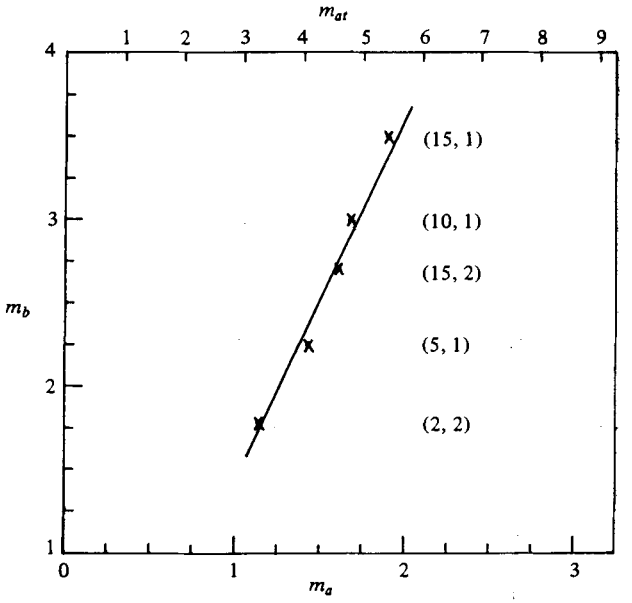

FIGURE 12. Pre-contraction decay slope, m_b, *vs.* post-contraction decay slope, m_a or m_{at}.

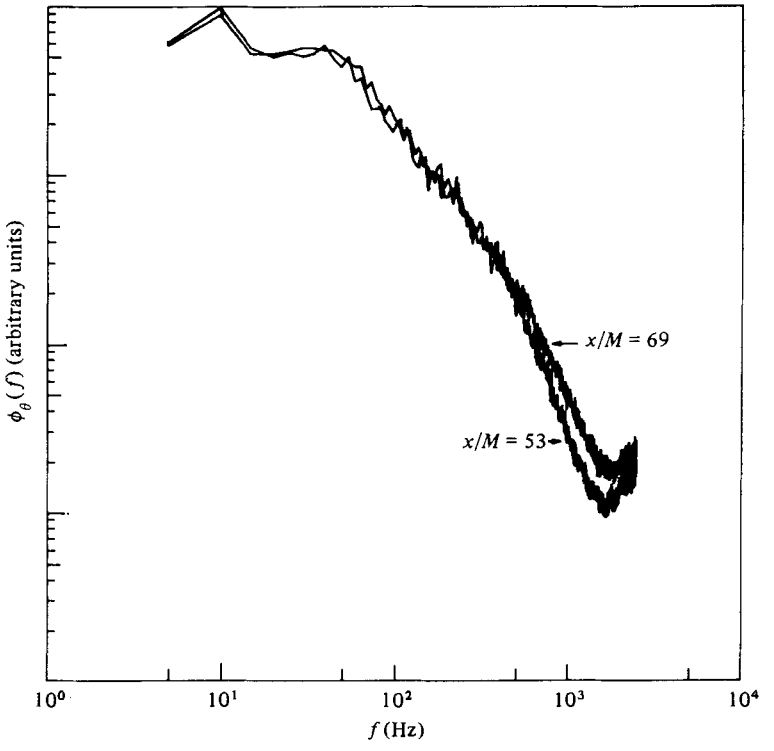

FIGURE 13. One-dimensional temperature spectra before and after the contraction for *mandoline* at (5, 1).

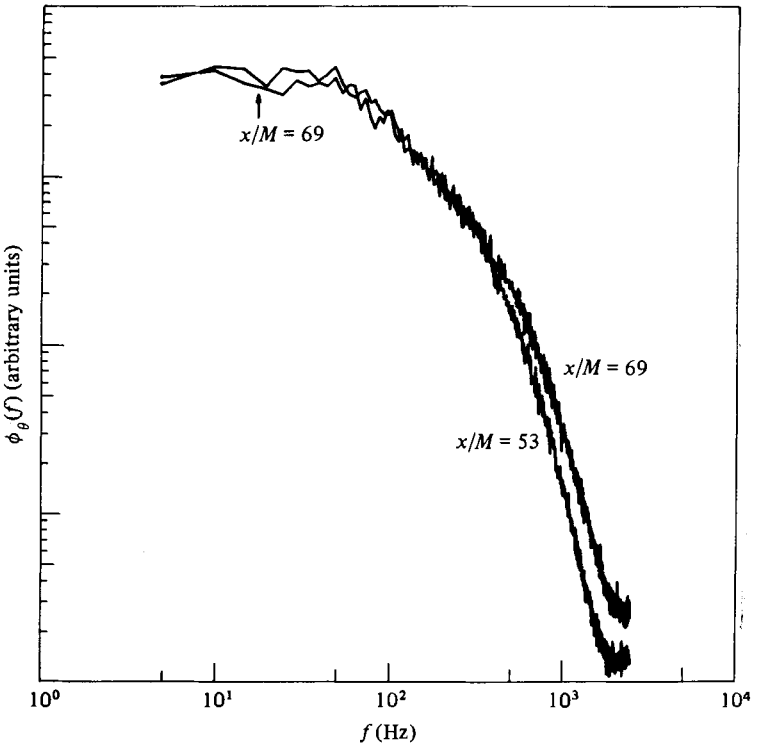

FIGURE 14. One-dimensional temperature spectra before and after the contraction for the *mandoline* at (10, 1).

spectrum according to the isotropic relation

$$E_\theta(k) = -\tfrac{1}{2}k\, d\phi_\theta(k)/dk.$$

Note, that for the *mandoline* at (15, 1) (fig. 16) a low-wavenumber peak appears in the three-dimensional spectrum. It is not clear why this occurs, but its energy is small compared with the high-frequency peak, the latter of which was used to define k_θ (table 1). Figure 17 shows the normalized three-dimensional pre-contraction temperature spectra. The scatter in the peaks is comparable to the scatter in the PSU data (Warhaft & Lumley, 1978*a*, figure 21). The difference in amplitude between the PSU spectra and those of figure 17 is due to the different length scales (deduced from the velocity decay laws) for the two sets of data.

As for the velocity data, in order to compare thermal-scale sizes before and after the contraction the one-dimensional temperature spectra were multiplied by k_1 and the resultant spectra are shown in figure 18 (before the contraction) and figure 19 (after the contraction). The one-dimensional spectra before the contraction (figure 18) are, of course, in conformity with the three-dimensional spectra at that location (figure 16) and march to higher wavenumbers as r increases. We show here that the same situation is maintained after the contraction: as the pre-contraction time-scale ratio is increased, the post-contraction spectra march to higher wavenumbers. Note that figures 18 and 19 are plotted in terms of local wavenumber and not frequency. Table 3 shows the wavenumbers of the pre-contraction one-dimensional temperature

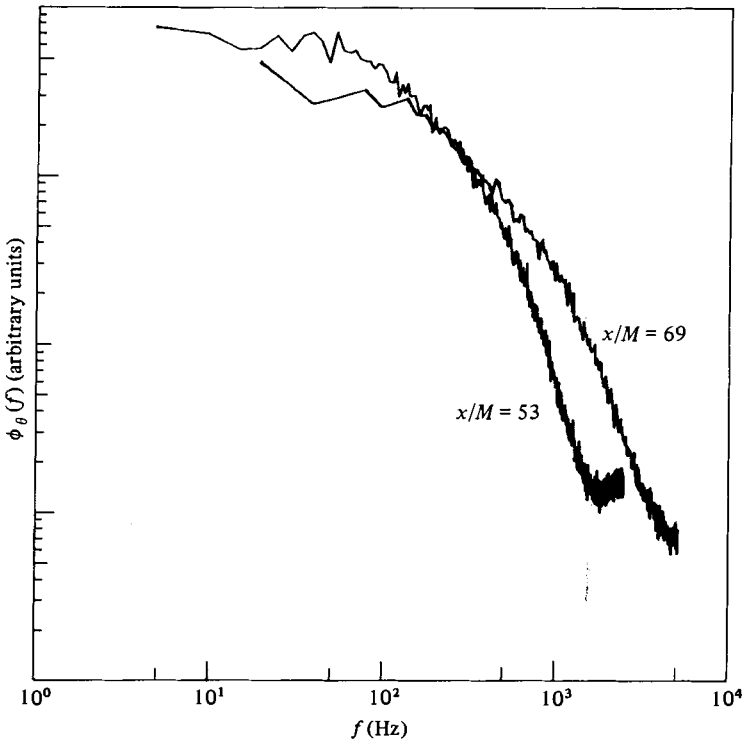

FIGURE 15. One-dimensional temperature spectra before and after the contraction for the *mandoline* at (15, 1).

spectrum peaks (k_b) and the post-contraction peaks (k_a) for the various *mandoline* experiments.

It is evident from figures 18 and 19 (and from figures 13, 14 and 15 from which they are derived) that k_b/k_a is not constant. Figure 20 in which k_b is plotted as a function of k_a suggests an approximate power-law relationship between k_a and k_b. The plot of figure 21, appears, however, to be more useful in comparing the pre- and post-contraction scale sizes. This figure is a plot of $k_b/k_{u,b}$, where $k_{u,b}$ is the peak of the one-dimensional pre-contraction velocity spectrum (from figure 6), as a function of k_b/k_a. $k_b/k_{u,b}$ is proportional to r. The figure suggests that if $k_b/k_{u,b}$ is approximately unity, i.e. if the scale size of the thermal and velocity fluctuations entering the contraction are comparable, then the contraction increases the length scale of the thermal fluctuations by approximately the contraction ratio, which is 4. However, if the ratio of the scale size of the thermal/velocity field is significantly less than unity ($k_b/k_{u,b} > 1$) then the contraction changes the length scale of the thermal field by much less than a factor of 4.

Figure 22 shows, for the post-contraction region, the variation with x/M of the one-dimensional temperature spectra for the *mandoline* at (2, 2) and (15, 1). Although the thermal field is rapidly decaying there appears to be a slight march of the one-dimensional spectra to higher wavenumbers, i.e. the thermal scale size appears to be decreasing. This tendency was observed for the other *mandoline* configurations. As for the one-dimensional v spectra, the reason for this is wanting.

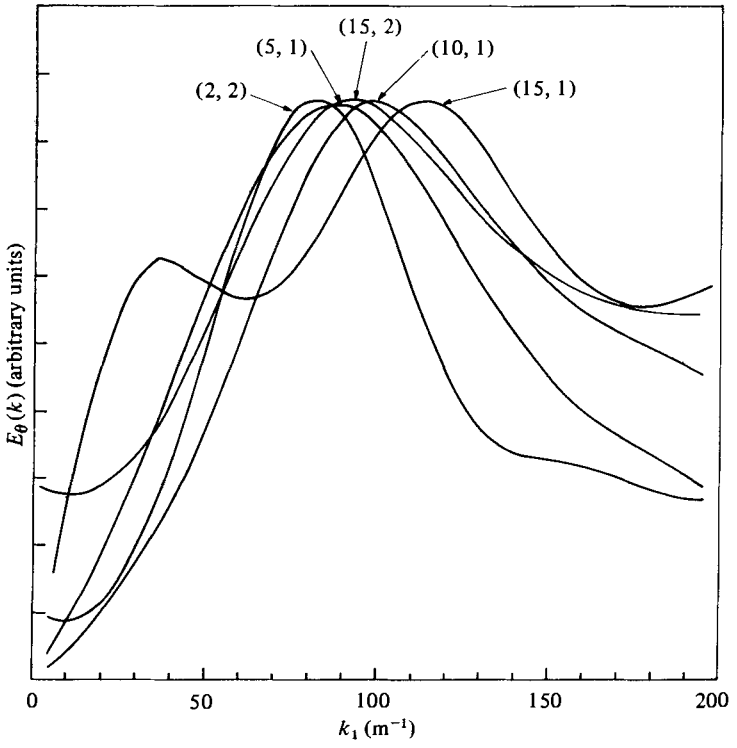

FIGURE 16. Three-dimensional temperature spectra at $x/M = 53$ for the five *mandoline* configurations. Arbitrary units have been used for the vertical axis in order to compare the wavenumbers at which each spectrum peaks (see table 1 for values).

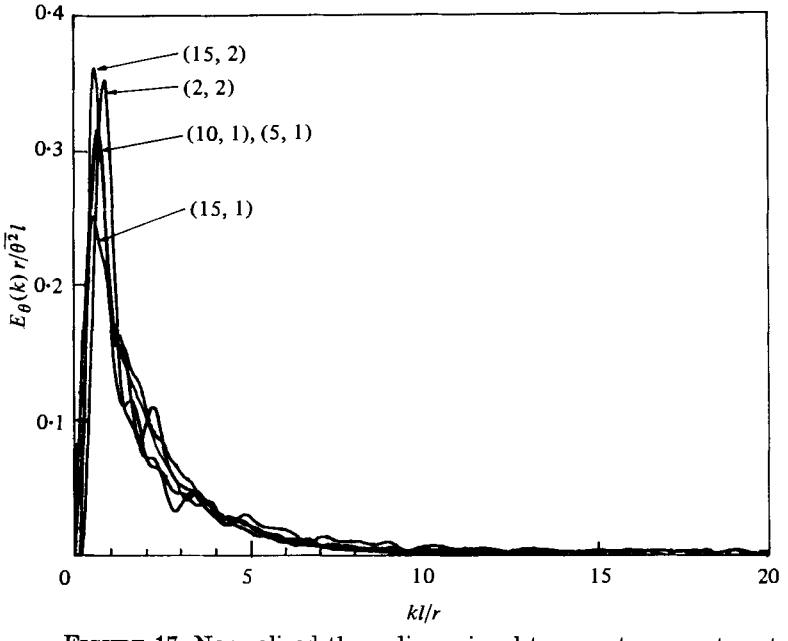

FIGURE 17. Normalized three-dimensional temperature spectra at $x/M = 53$ for the five *mandoline* configurations.

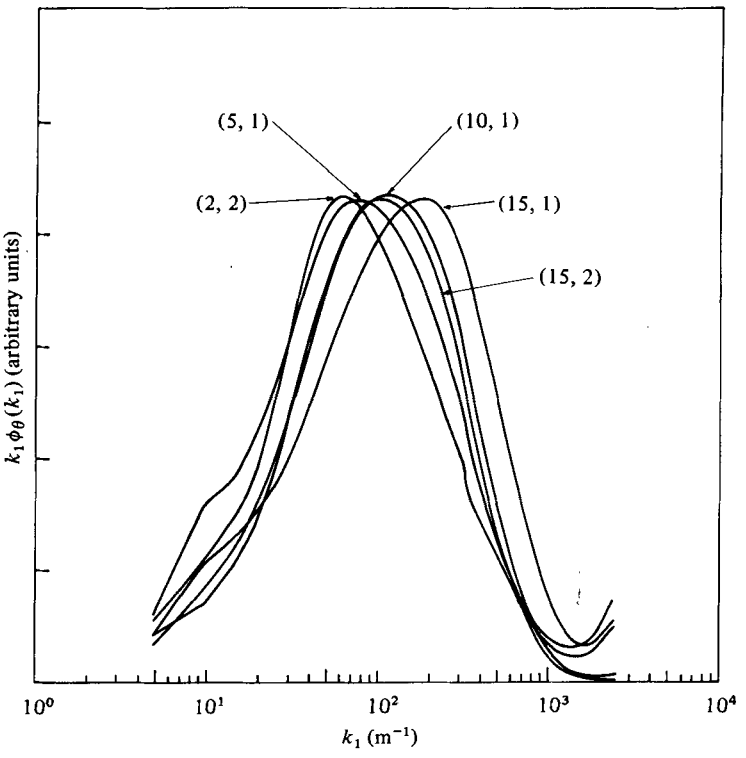

FIGURE 18. One-dimensional temperature spectra at $x/M = 53$ for the five *mandoline* configurations (pre-contraction).

4.2(c) *Cross-correlation and coherence characteristics.* In §4.2(*a*) it was shown that the decay exponents for the temperature variance, both before and after the contraction, are insensitive to the initial thermal fluctuation intensity. Here we will examine the effect of changing the initial *mandoline* heating on $\rho_{u\theta}$. Figure 23 shows $\rho_{u\theta}$ as a function of x/M for four different *mandoline* configurations: (10, 1), (5, 1), (2, 2) and (1, 2). The latter case (1, 2) has not been previously discused since m_a, m_b, k_a and k_b were the same as for the case (2, 2); i.e. the spectral and decay characteristics were the same as for the *mandoline* at (2, 2). For all the experiments of figure 23 the thermal field was experimentally determined to be a passive additive.

Figure 23 exhibits two striking characteristics. First, the contraction induces significant post-contraction cross-correlation even if the pre-contraction value is small. Second, $\rho_{u\theta}$ tends toward zero relatively fast in the post-contraction region. We will return to this point below.

Figure 24, a plot of the u, θ coherence, $|\phi_{u\theta}(k_1)|^2/\phi_u(k_1)\,\phi_\theta(k_1)$, for the *mandoline* at (10, 1) and with a current of 2·4 A, shows that the post-contraction coherence is peaked at low wavenumbers, i.e. at wavenumbers in the energy-containing region of the thermal spectrum (figure 19) and at lower wavenumbers than the energy-containing region of the post-contraction velocity spectrum (figure 7). Note that the pre-contraction coherence is negligible for this case. Figure 25 shows the effect of increasing the initial temperature fluctuation intensity. Again, this is for the *mandoline*

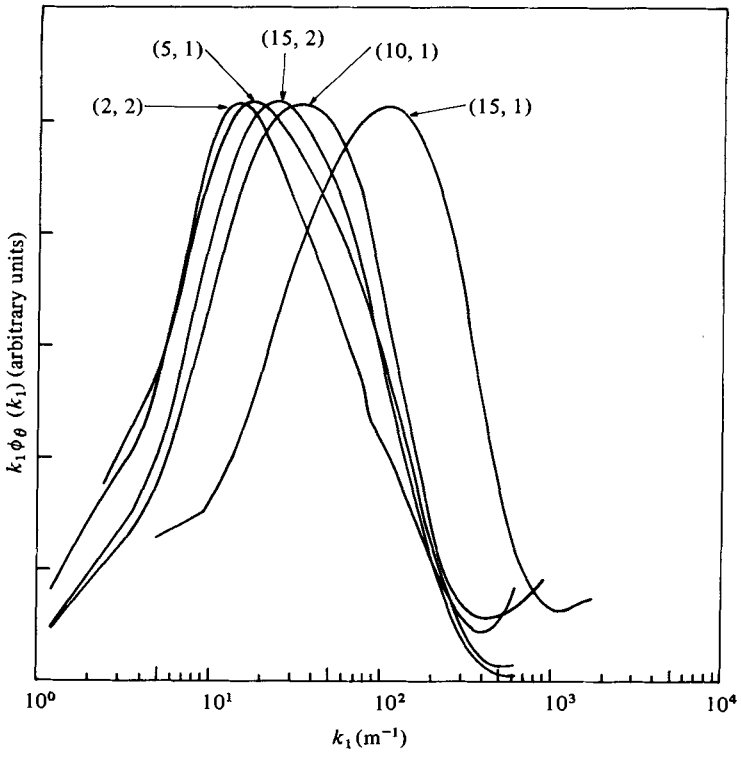

FIGURE 19. One-dimensional temperature spectra at $x/M = 69$ for the five *mandoline* configurations (post-contraction).

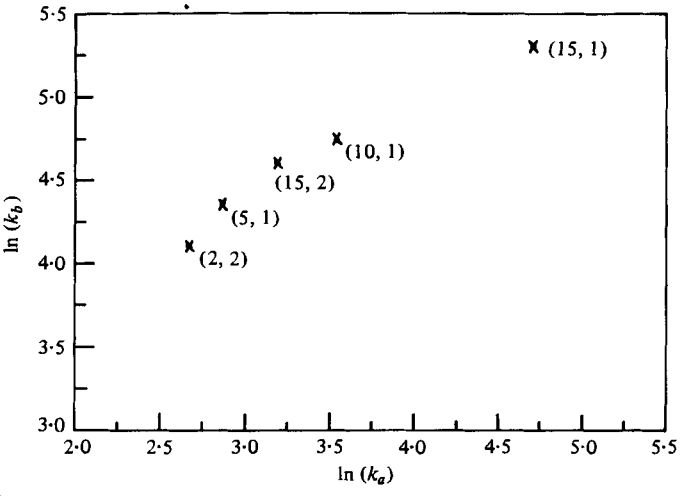

FIGURE 20. The peaks of the pre-contraction one-dimensional temperature spectra k_b (from figure 18) *vs.* the peaks of the post-contraction one-dimensional temperature spectra k_a (from figure 19).

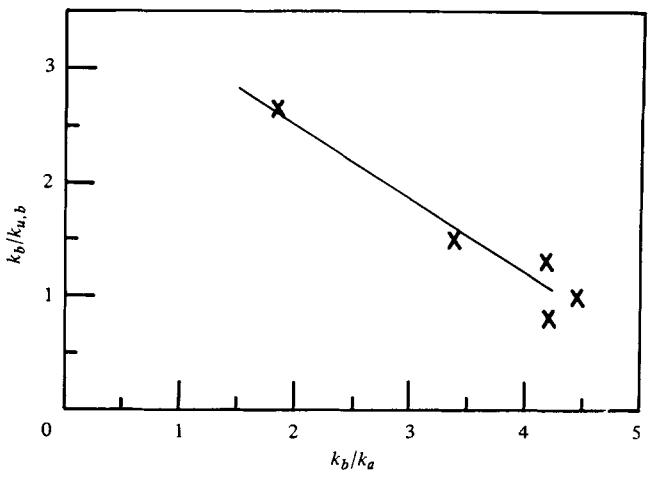

FIGURE 21. The ratio of the peak of the one-dimensional pre-contraction temperature spectrum to the peak of the one-dimensional pre-contraction velocity spectrum *vs.* the ratio of the pre- and post-contraction peaks of the one-dimensional temperature spectra.

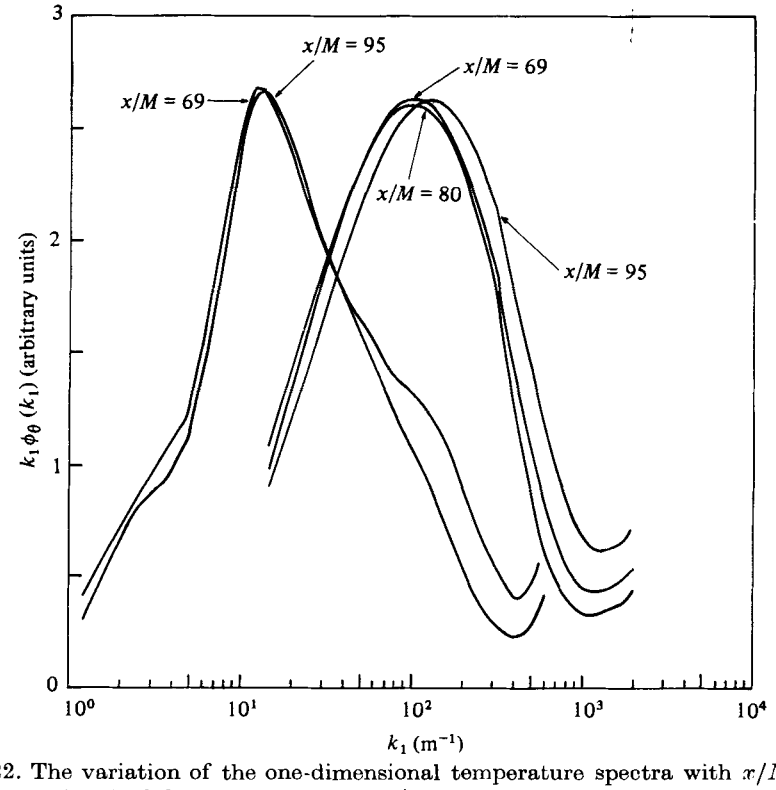

FIGURE 22. The variation of the one-dimensional temperature spectra with x/M in the post-contraction region. Left-hand set of curves (x/M = 69, 95), *mandoline* at (2, 2); right-hand set of curves (x/M = 69, 80, 95), *mandoline* at (15, 1).

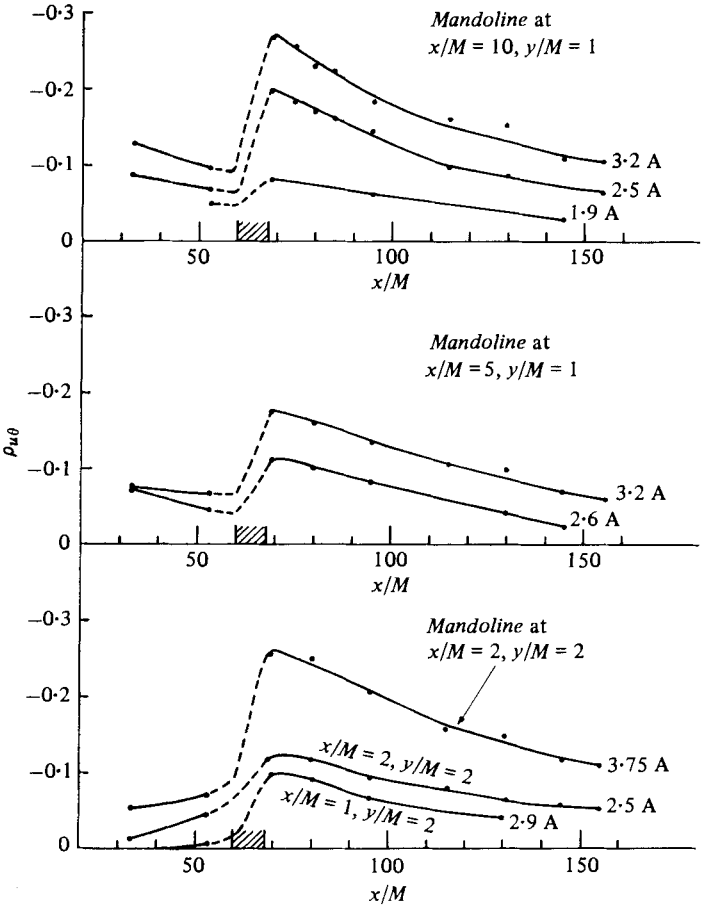

FIGURE 23. The cross-correlation between u and θ as a function of x/M for various *mandoline* configurations and heating currents.

at (10, 1), but with 3·2 A. For this case too the pre-contraction coherence (not shown) was also essentially zero.

Finally we examine the cross-correlation and coherence for the *mandoline* at (15, 2) for high initial thermal fluctuations, i.e. for the high heating of figure 11. Figure 26 shows that for this run the pre-contraction $\rho_{u\theta}$ was $-0{\cdot}4$ and rose to nearly $-0{\cdot}8$ after passing through the contraction. This strong post-contraction correlation induced buoyancy: at $x/M = 69$ the r.m.s. of u was approximately 30% greater than for the experiments done with low thermal fluctuations (or for no thermal fluctuations at all) and decreased to 10% above that of the non-buoyant case at $x/M = 115$. Significant buoyancy effects were not present, however, in the pre-contraction region. $\rho_{u\theta}$ is plotted as a function of dimensionless time as well as a function of x/M in figure 26. The former variable is to be used when comparing the contraction decay with the $\rho_{u\theta}$ decay done without the contraction which is also shown in this figure.

It is evident that the strong correlation inducted by the contraction tends towards zero with great haste, at least initially. Although figure 26 suggests that $\rho_{u\theta}$ decays faster for the anisotropic turbulence than for the isotropic turbulence (without

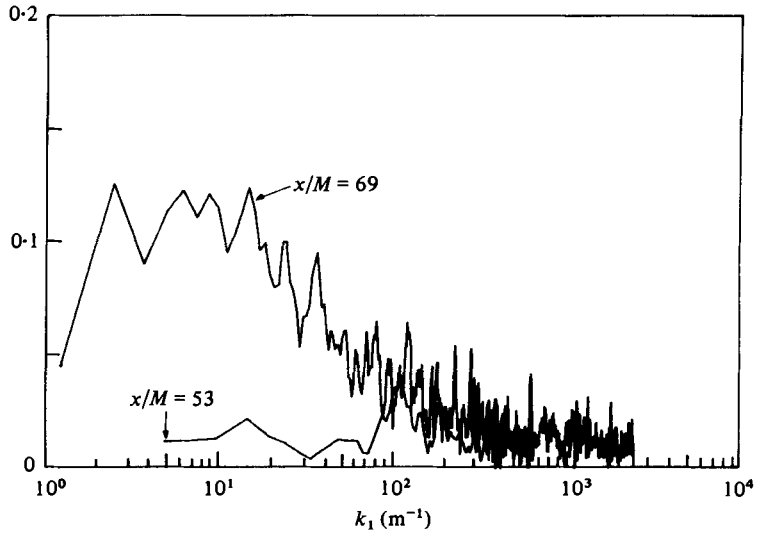

FIGURE 24. The coherence of u and θ before and after the contraction for the *mandoline* at (10, 1), 2·6 A heating current.

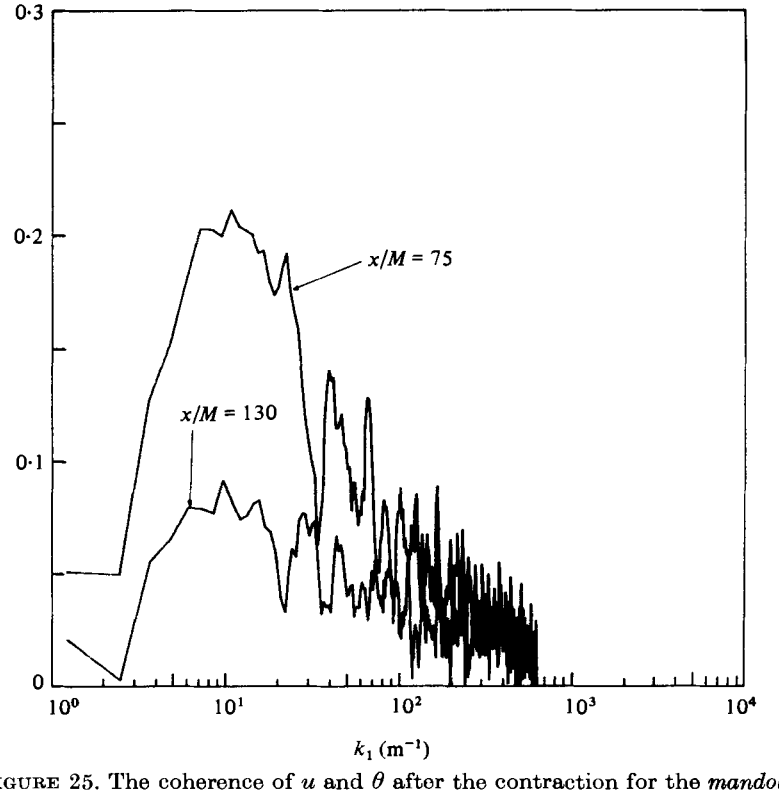

FIGURE 25. The coherence of u and θ after the contraction for the *mandoline* at (10, 1), 3·2 A heating current.

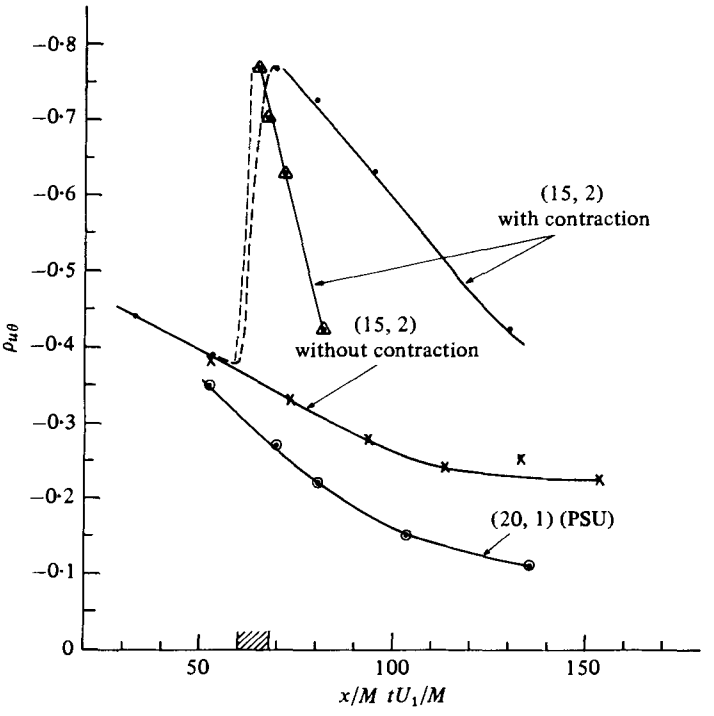

FIGURE 26. The cross-correlation between u and θ for the *mandoline* at (15, 2), and high (4·5 A) heating: •, as a function of x/M; △, as a function of tU_1/M. ×, the same *mandoline* heating but without the contraction; ⊙, earlier PSU results for the *mandoline* at (20, 1) (see Warhaft & Lumley 1978*b*).

contraction) comparison of the two cases of figure 26 may be misleading since the decay rate of $\rho_{u\theta}$ may be a function of its initial value, i.e. a high initial magnitude of $\rho_{u\theta}$ may decay at a greater rate than a lower initial value. However, the post-contraction cross-correlations of figure 23 are of comparable magnitude to those of the isotropic case of figure 26 and a comparison of these, if the former are plotted in terms of dimensionless time, shows that $\rho_{u\theta}$ does in fact decay at a faster rate for the axisymmetric case than for the isotropic case. We note that Lumley (1978) used second-order modelling procedures to examine $d\rho_{u\theta}/dt$ in both isotropic and in axisymmetric homogeneous turbulence and his analysis suggest that the decay of $\rho_{u\theta}$ should depend on the degree of anisotropy.

Also plotted in figure 26 is an earlier $\rho_{u\theta}$ decay done in the PSU tunnel (Warhaft & Lumley 1978*b*) for initial $\rho_{u\theta}$ of comparable magnitude to the present trial but with the mandoline at (20, 1). The $\rho_{u\theta}$ decay is slightly faster than for the *mandoline* at (15, 2) (without the contraction) and this may be due to the higher value of r which was 2·39 for the PSU measurement and 1·8 for the *mandoline* at (15, 2).

Figure 27 shows the coherence both before and after the contraction as a function of local wavenumber, for the *mandoline* at (15, 2) and with the high heating. The pre-contraction coherence is now significant and relatively flat (cf. Warhaft & Lumley 1978*b*, figure 8). The post-contraction coherence is initially high and single-peaked and is comparable in form to the initial post-contraction coherence for lower heating

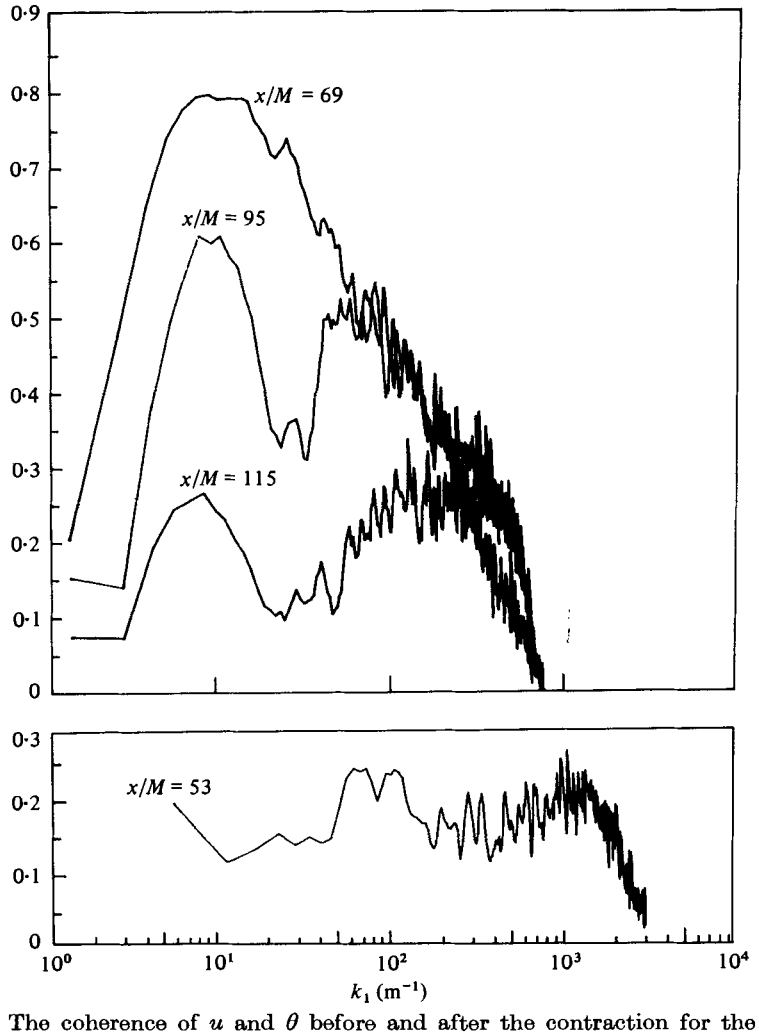

FIGURE 27. The coherence of u and θ before and after the contraction for the *mandoline* at (15, 2) and high (4·5 A) heating. All plots are a function of local wavenumber.

(figures 24 and 25). Note, however, that, as the thermal field decays, the coherence becomes double-peaked. A spectral gap divides the coherence into a low-frequency peak, of wavenumber range about the same as the peak in the temperature spectrum (figure 19) and a high-frequency peak which is at about the same wavenumber as the peak in the velocity spectrum (figure 7).

5. Concluding remarks

The finding that the contraction does not cause the thermal fluctuation decay rate to equilibrate to a constant value is consistent with the effect the strain has on the thermal length scale, i.e. the post-contraction thermal length scale is determined by the pre-contraction thermal length scale. Thus, as was found by Warhaft & Lumley (1978*a*) for isotropic turbulence, the decay rate of thermal fluctuations in homogeneous

axisymmetric turbulence appears to be a unique function of the initial (post-contraction) thermal length scale.

The remarkable effect that the contraction has in inducing strong correlation between the velocity and temperature fluctuations, and hence significant heat flux, as well as the evolution of the thermal and velocity scale sizes under the action of the strain, requires analytical study. For example, it is not clear whether a residual negative $\rho_{u\theta}$ must exist before the contraction for the contraction to induce the large negative $\rho_{u\theta}$. Figure 23 shows some examples where the pre-contraction $\rho_{u\theta}$ is very small, but never zero. Further, if by some means $\rho_{u\theta}$ before the contraction could be made positive, would the contraction amplify this, as it appears to do for the negative correlation? Further, what would be the effect of straining on a thermal field with $r < 1$?

The results of the decay of the heat flux in the post-contraction region should provide insight into the problem of the return to isotropy of heat flux and thus lead to a better understanding of how to model the scalar-pressure gradient correlation term in the heat-flux equation.

Finally, we still do not have experimental evidence for an equilibrium value of the mechanical/thermal time-scale ratio in decaying turbulence and in this sense we are no closer to the objective of the previous experiment of Warhaft & Lumley (1978*a*). Indeed, the question may be asked: What must be done to the thermal field to cause it to equilibrate?

The study had its origin in my earlier collaboration with Dr J. L. Lumley. I thank him for his encouragement and advice. I also thank Mr E. P. Jordan for his enthusiastic technical assistance and Ms E. Terry for her careful help with the measurements. This work is supported by the U.S. National Science Foundation, Meteorology Program under grant no. ATM77-22903.

REFERENCES

BATCHELOR, G. K. 1953 *The Theory of Homogeneous Turbulence*. Cambridge University Press.

COMTE-BELLOT, G. & CORRSIN, S. 1966 The use of a contraction to improve the isotropy of grid generated turbulence. *J. Fluid Mech.* **25**, 657–682.

HERRING, J. R. & NEWMAN, G. R. 1979 A test field model study of a passive scalar in isotropic turbulence. Paper presented at *2nd Symp. on Turbulent Shear Flows, Imperial College, London.*

KRAICHNAN, R. H 1959 The Structure of isotropic turbulence at very high Reynolds numbers. *J. Fluid Mech.* **5**, 497–543.

LUMLEY, J. L. 1978 Computational modeling of turbulent flows. *Adv. Appl. Mech.* **18**, 123–176.

LUMLEY, J. L. & NEWMAN, G. R. 1977 The return to isotropy of homogeneous turbulence. *J. Fluid Mech.* **82**, 161–178.

LUMLEY, J. L. & PANOFSKY, H. A. 1964 *The Structure of Atmospheric Turbulence*. Wiley-Interscience.

MILLS, R. R. & CORRSIN, S. 1959 Effects of contraction on turbulence and temperature fluctuations generated by a warm grid. *N.A.S.A. Memo.* no. 5-5-59W.

NEWMAN, G. R. & HERRING, J. R. 1979 A test field model study of a passive scalar in isotropic turbulence. *J. Fluid Mech.* **94**, 163–194.

PRANDTL, L. 1933 Attaining a steady air stream in wind tunnels. *N.A.C.A. Tech. Memo.* no. 726.

RIBNER, H. S. & TUCKER, M. 1952 Spectrum of turbulence in a contracting stream. *N.A.C.A. Tech. Note* no. 2606.

ROTTA, J. 1951 Statistische Theorie nichthomogener Turbulenz. *Z. Phys.* **129**, 547–572.

SCHUMANN, U. & HERRING, J. R. 1976 Axisymmetric homogeneous turbulence: A comparison of direct spectral simulations with the direct-interaction approximation. *J. Fluid Mech.* **76**, 755–782.

SCHUMANN, U. & PATTERSON, G. S. 1978 Numerical study of the return of axisymmetric turbulence to isotropy. *J. Fluid Mech.* **88**, 711–736.

TAYLOR, G. I. 1935 Turbulence in a contracting stream. *Z. angew. Math. Mech.* **15**, 91–6. (Also *Collected Works* (ed. G. K. Batchelor), Cambridge University Press, 1960.)

TENNEKES, H. & LUMLEY, J. L. 1972 *A First Course in Turbulence.* Massachusetts Instutite of Technology Press.

UBEROI, M. S. 1956 Effect of wind-tunnel contraction on free stream turbulence. *J. Aero. Sci.* **23**, 754–764.

WARHAFT, Z. & LUMLEY, J. L. 1978*a* An experimental study of the decay of temperature fluctuations in grid-generated turbulence. *J. Fluid Mech.* **88**, 659–684.

WARHAFT, Z. & LUMLEY, J. L. 1978*b* The decay of temperature fluctuations and heat flux in grid-generated turbulence. In *Structure and Mechanisms of Turbulence II* (ed. H. Fiedler), Lecture notes in Physics, vol. 76, pp. 113–123. Springer.

YEH, T. T. & VAN ATTA, C. W. 1973 Spectral transfer of scalar and velocity fields in heated grid turbulence. *J. Fluid Mech.* **58**, 233–261.